Acta Crystallographica Section B
Structural Science
ISSN 0108-7681

$(111)_p$ microtwinning in $SrRuO_3$ thin films on $(001)_p$ $LaAlO_3$

Y. Han,[a]* I. M. Reaney,[a] D. S. Tinberg[b] and S. Trolier-McKinstry[b]

[a]Department of Engineering Materials, University of Sheffield, Sir Robert Hadfield Building, Mappin Street, Sheffield S1 3JD, England, and [b]Materials Research Institute and Materials Science and Engineering Department, Pennsylvania State University, University Park, Pennsylvania 16802, USA

Correspondence e-mail: y.han@sheffield.ac.uk

Received 28 September 2009
Accepted 28 October 2009

$SrRuO_3$ (SRO) thin films grown on $(001)_p$ (p = pseudocubic) oriented $LaAlO_3$ (LAO) by pulsed laser deposition have been characterized using transmission electron microscopy. Observations along the $\langle 100\rangle_p$ directions suggests that although the SRO layer maintains a pseudocube-to-pseudocube orientation relationship with the underlying LAO substrate, it has a ferroelastic domain structure associated with a transformation on cooling to room temperature to an orthorhombic *Pbnm* phase ($a^-a^-c^+$ Glazer tilt system). In addition, extra diffraction spots located at $\pm 1/6(ooo)_p$ and $\pm 1/3(ooo)_p$ (where 'o' indicates an index with an odd number) positions were obtained in $\langle 110\rangle_p$ zone-axis diffraction patterns. These were attributed to the existence of high-density twins on $\{111\}_p$ pseudocubic planes within the $SrRuO_3$ films rather than to more conventional mechanisms for the generation of superstructure reflections.

1. Introduction

$SrRuO_3$ (SRO) is widely used as a bottom electrode for perovskite thin films due to its metallic electrical conductivity, high resistance to chemical erosion and good lattice matching with a wide range of perovskite materials (Eom *et al.*, 1992; Lee *et al.*, 2004, 2005). At room temperature, it has a $GdFeO_3$-type orthorhombic structure (space group *Pbnm*), which can be described as a distorted pseudocubic perovskite cell with $a = a_p\sqrt{2}$, $b = a_p\sqrt{2}$ and $c = 2a_p$ ($a_p \simeq 3.93$ Å, where p denotes pseudocubic; Kennedy & Hunter, 1998). The *Pbnm* symmetry of SRO is dictated by an $a^-a^-c^+$ Glazer tilt system (Glazer, 1972), in which the O octahedra rotate with equal magnitude in antiphase around the a_p and b_p axes and in-phase around c_p.

Epitaxial SRO has been successfully grown on (001)-oriented substrates including Si (Chen *et al.*, 2002; Oh & Park, 2001), MgO (Ai *et al.*, 2006; Fahey *et al.*, 1995), $(LaAlO_3)_{0.3}$–$(SrAl_{0.5}Ta_{0.5}O_3)_{0.7}$ (LSAT; Takahashi *et al.*, 2002), $LaAlO_3$ (Jiang & Pan, 2001; Vasco *et al.*, 2003) and $SrTiO_3$ (Takahashi *et al.*, 2002; Fahey *et al.*, 1995; Chen *et al.*, 1997; Jiang *et al.*, 1998; Gan *et al.*, 1998; Maria *et al.*, 2000; Bachelet *et al.*, 2008; Oh & Park, 2004; Zakharov *et al.*, 1999), by techniques such as pulsed-laser deposition (PLD), ion-beam sputtering, *rf* magnetron sputtering or metallorganic chemical vapour deposition (MOCVD). The ferroelastic domain structure of thin-film SRO is now well understood. Even though the SRO layer maintains a well defined pseudocube-on-pseudocube epitaxial relationship with the underlying substrates, ferroelastic domain structures are generally observed (Ai *et al.*, 2006; Fahey *et al.*, 1995; Chen *et al.*, 2002; Herranz *et al.*, 2005; Jiang & Pan, 2001). These domains arise due to the transformation on cooling to an orthorhombic *Pbnm* structure with the $a^-a^-c^+$ Glazer tilt system. Additionally, the defect struc-

© 2009 International Union of Crystallography
Printed in Singapore – all rights reserved

ture of SRO thin films grown on (001)-oriented $SrTiO_3$ has been studied by TEM. SRO layers form pure edge-type dislocations at the SRO/STO interface to relieve misfit strain (Oh & Park, 2004). Antiphase boundaries, ferroelastic twins and point defects have also been reported and are considered to be responsible for a reduction in conductivity (Zakharov *et al.*, 1999). Here, we explore the twinning arrangements related to growth defects in SRO grown on $LaAlO_3$ substrates.

2. Experimental procedure

$SrRuO_3$ epitaxial films were deposited on $(001)_p$-oriented $LaAlO_3$ substrates for $\sim$ 10 min using pulsed laser deposition. The substrates were obtained from MTI Crystal Inc. (Richmond, CA). Prior to deposition, the substrates were cleaned in an ultrasonic bath by successive immersion in acetone, methanol and isopropanal, followed by drying using an Ar gas stream. A KrF laser (Lambda Physik Compex 102, Fort Lauderdale, FL) was used to ablate material from a $SrRuO_3$ target (Target Materials, Inc., Columbus, OH), using a laser energy density of ~ 2 J cm^{-2}. Films were grown using a substrate temperature of 953 K in 160 mTorr of O_2/O_3, at a target to substrate distance of 8 cm, as described elsewhere (Maria *et al.*, 1998).

In addition, $SrRuO_3$ ceramics were prepared by a conventional mixed-oxide route. Stoichiometrically mixed high-purity powders of $SrCO_3$ (99.95%) and RuO_2 (99.9%) were wet milled for 24 h and then calcined for 12 h at 1273 K. Pellets 6 mm in diameter were uniaxially pressed at 110 MPa into discs and sintered for 12 h at 1423 K.

Cross-sectional TEM specimens for the $SrRuO_3$ epitaxial films and TEM thin foils for the $SrRuO_3$ pellets were prepared by standard mechanical polishing followed by Ar-ion milling using a Gatan Duo Mill, operated at 6 kV and a combined current of 6 mA. Microstructural characterization was performed using diffraction-contrast imaging, phase-contrast imaging and selected-area electron diffraction techniques using a Jeol 2010f transmission electron microscope (TEM), operated at 200 kV. In this context, all crystallographic directions and planes refer to the pseudocubic unit cell.

3. Results and discussion

The SRO/LAO(001) samples were examined by X-ray diffraction using θ–2θ and φ scans, which confirmed the typical pseudocube-on-pseudocube orientation relationship between the SRO layer and the LAO substrate (Ai *et al.*, 2006; Takahashi *et al.*, 2002; Chen *et al.*, 1997; Gan *et al.*, 1998). Fig. 1 is a dark-field image taken from the SRO/LAO(001) sample using one of the $\{110\}_p$ spots close to the $\langle 001\rangle$ pseudocubic direction. The film is $\sim$ 60 nm thick and highly faulted/strained, as evidenced by the strong and varied diffraction contrast under two-beam conditions.

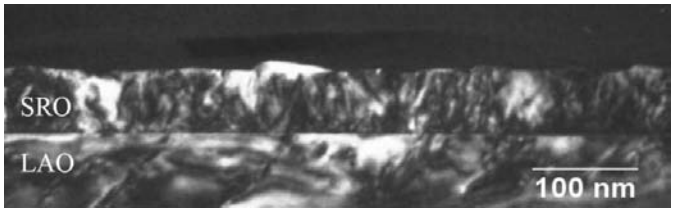

Figure 1
Dark-field image from the SRO/LAO(001) sample taken along a $\langle 100\rangle$ pseudocubic direction.

For comparison, electron-diffraction patterns were also recorded from a bulk ceramic SRO sample. Figs. 2(*a*), (*b*) and (*c*) are representative diffraction patterns from the bulk SRO taken along the [001], [100] and [110] zone axes, respectively. In addition to fundamental diffraction spots, superlattice reflections are also present at $\frac{1}{2}\{ooe\}$ ($h \neq k$), $\frac{1}{2}\{ooo\}$ ($h \neq k$) and $\frac{1}{2}\{eeo\}$ ($h \neq k$) positions (where {ooe} represents a general form of Miller indices with 'o' indicating an index with an odd number and 'e' with an even number), in agreement with the known *Pbnm* symmetry and $a^-a^-c^+$ Glazer tilt system (Kennedy & Hunter, 1998; Glazer, 1972). Diffraction patterns

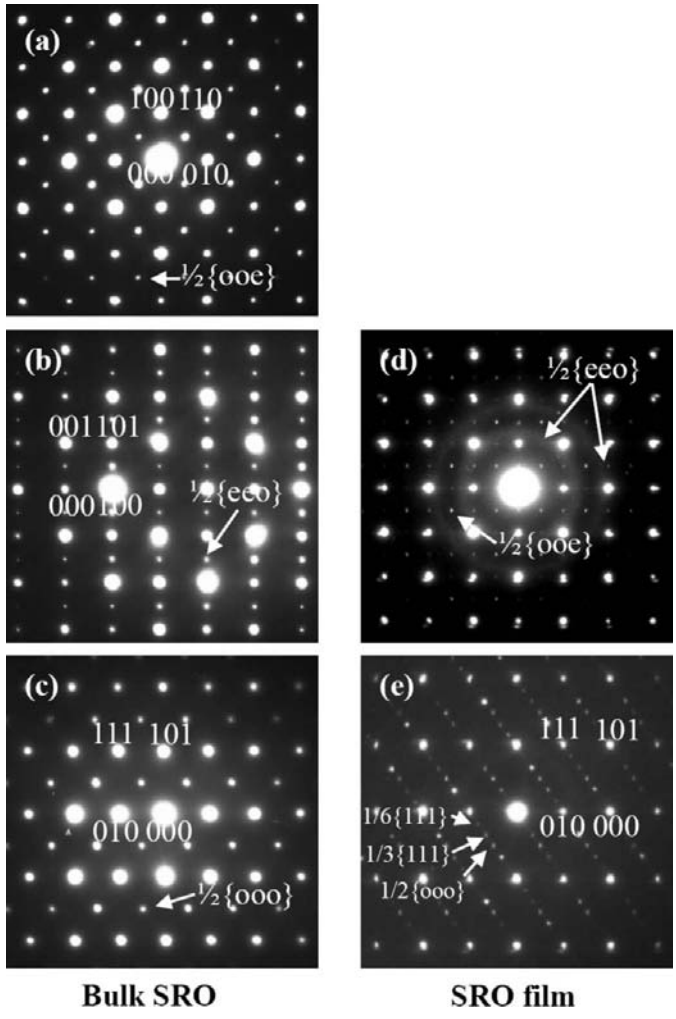

Figure 2
(*a*), (*b*) and (*c*) diffraction patterns taken from bulk SRO ceramics along the $\langle 001\rangle$, $\langle 100\rangle$ and $\langle 110\rangle$ pseudocubic axes; (*d*) and (*e*) are diffraction patterns taken from the SRO/LAO thin films along the $\langle 100\rangle$ and $\langle 110\rangle$ pseudocubic axes.

taken from the SRO film on LAO(001) along the ⟨100⟩ and ⟨110⟩ pseudocubic directions are shown in Figs. 2(*d*) and (*e*). Fig. 2(*d*) is a diffraction pattern in which three sets of superlattice reflections (two sets of the type $\frac{1}{2}${ooo} and one set of the type $\frac{1}{2}${eeo}) associated with three ⟨100⟩ pseudocubic zone axes are recorded. Such $\langle 100\rangle_p$ projection diffraction patterns suggest that the SRO layer is multi-domain. However, in contrast with the bulk electron-diffraction data, extra spots are also located at ±1/6(ooo) and ±1/3(ooo) positions along the $\langle 110\rangle_p$ projections (arrowed in Fig. 2*e*).

In Fig. 3 the diffraction pattern in Fig. 2(*e*) is reconstructed from (111) twinned single domain variants of the pseudocubic ⟨110⟩ zone axis. The superstructure reflections at ±1/6(ooo) and ±1/3(ooo) positions are reproduced and attributed to either (111) SRO twins or multiple diffraction effects. The dark and red circles correspond to the fundamental diffraction spots from the cube-on-cube epitaxial SRO (denoted as 'matrix SRO') and the twins with solid circles corresponding to the $\frac{1}{2}${ooo} superlattice spots for each case.

A simulation of the [110] zone-axis diffraction pattern from the matrix is shown in Fig. 3(*a*). The equivalent zone-axis diffraction pattern from across the twin is rotated at ∼ 70.7° with respect to that from the matrix, Fig. 3(*b*). When Figs. 3(*a*) and (*b*) are superimposed, it is evident that the major effect of the twin operation is to produce systematic rows of diffraction spots at some but not all ±1/6(ooo) and ±1/3{ooo} positions, Fig. 3(*c*). The electron beam is parallel to the (111) twin plane and the diffraction patterns from the matrix and the twins are mirror reflections. However, some spots at ±1/3(111) positions are absent in Fig. 3(*c*). If some likely generic double diffraction routes are taken into account, *e.g.* (ooo) ± 1/3(ooo) = ±2/3(ooo), reflections may appear at nominally absent ±1/3{ooo} positions, as illustrated in Fig. 3(*d*). In thinner regions of the sample where kinematic conditions dominate, the double diffracted reflections are considerably weaker and the experimental pattern, Fig. 3(*e*), shows a strong correlation with the simulation shown in Fig. 3(*c*) (kinematic only). In thicker regions where dynamical conditions dominate, the experimental pattern, Fig. 3(*f*), resembles closely the simulation in Fig. 3(*d*), which includes some likely doubly diffracted spots.

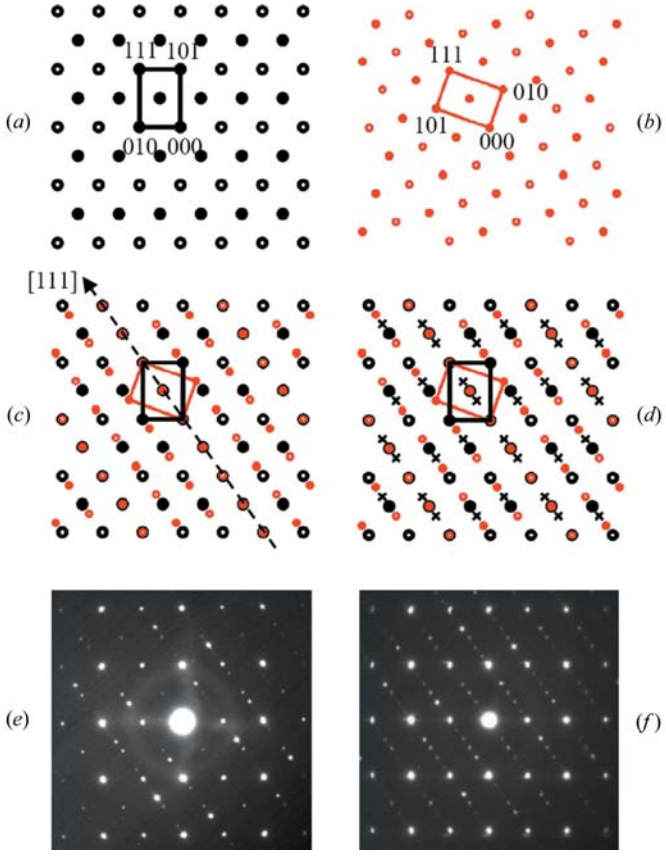

Figure 3
Schematic SRO ⟨110⟩ zone-axis diffraction patterns from (*a*) the matrix and (*b*) a twin which when superimposed give rise to (*c*). (*d*) Identical schematic to (*c*) which also includes some reflections (indicated by crosses) generated by multiple diffraction. (*e*) and (*f*) Experimental zone-axis diffraction patterns from thin and thick regions of the TEM foil that match schematics (*c*) and (*d*). This figure is in colour in the electronic version of this paper.

Fig. 4(*a*) is a dark-field image recorded using a diffraction spot attributed to the microtwins, *i.e.* one of the red circles located at ±1/3{ooo} positions in Fig. 3(*c*), in which an inclined twin grain is highlighted. The width of the twin is ∼ 30 nm. Fig. 4(*b*) is a high-resolution image, which shows an inclined twin structure and sharp (111) twin/matrix boundaries. In addition, (111) twinning takes place on all four inclined {111} planes in this sample, giving rise to the diffraction pattern shown in Fig.

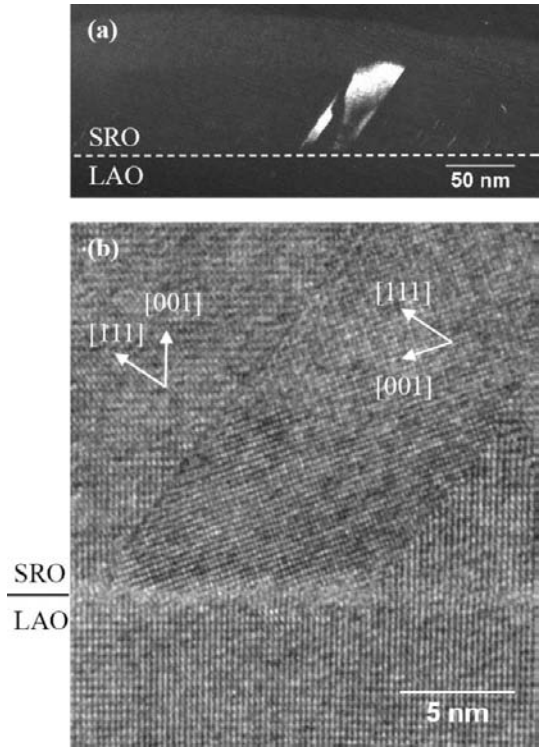

Figure 4
(*a*) Dark-field image from a region of the SRO/LAO(001) thin film, formed using a fundamental diffraction spot from twin grains. (*b*) High-resolution image showing an inclined twin structure and sharp (111) twin/matrix boundaries.

5 (which exhibits superstructure reflections along all ⟨111⟩ pseudocubic directions). The SRO layers also contain a high-density of stacking faults on (111) planes, with a representative high-resolution image shown in Fig. 6.

Initial interpretation of these reflections as arising from a twinned microstructure was problematic. In electron-diffraction patterns across the twin boundary, the fundamental and superstructure reflections are coincident with those previously reported in either hexagonal $BaTiO_3$ (Feteira *et al.*, 2006; Akimoto *et al.*, 1994), $BaTiO_3$-based ceramics with ordered $V_o^{\cdot\cdot}$ (Woodward *et al.*, 2004) or some tilted complex perovskites (Levin *et al.*, 2000). This is particularly true in thicker regions of the sample where dynamical diffraction conditions 'fill in' the salient systematic absences at $\pm1/3\{ooo\}$ and even $\pm1/6\{ooo\}$ positions which would normally be the fingerprint of a diffraction pattern arising from a twinned microstructure. Hexagonal $BaTiO_3$ contains face-shared O octahedra each third layer of O ions, which creates a unit cell in which reflections appear at $\pm1/6\{ooo\}$ positions (Feteira *et al.*, 2006; Akimoto *et al.*, 1994). However, all crystallographic data revealed the film to be pseudocubic rather than a hexagonal $BaTiO_3$ isomorph. Planes of $V_o^{\cdot\cdot}$ on each third (111) plane have also been shown to give rise to superlattice reflections at $\pm1/3(ooo)$ in $BaTiO_3$-based ceramics (Woodward *et al.*, 2004), which in combination with an $a^-a^-c^+$ tilt system could give rise to reflections at $\pm1/6\{ooo\}$ positions (Levin *et al.*, 2000). However, such a superstructure would be visible in all diffraction patterns taken throughout the film rather than only in those from regions which contain planar defects. Consequently, these alternative mechanisms for the formation of superstructure reflections at $\pm1/3\{ooo\}$ and $\pm1/6\{ooo\}$ positions were eliminated.

Growth twins within perovskite-structured ceramics have long been recognized (White *et al.*, 1985; Keller & Buseck, 1994; Wang & Lu, 2006; Feng & McConville, 2004; Chen *et al.*, 2002; Fahey *et al.*, 1995). In particular, the formation of (111) growth twins in $BaTiO_3$ bulk ceramics have been extensively investigated (Jugle, 1966; Eibl *et al.*, 1988; Oppolzer & Schmelz, 1983; Lee *et al.*, 2000; Krasevec *et al.*, 1990; Recnik *et al.*, 1994). Early studies suggested that highly (111) twinned microstructures can be obtained in $BaTiO_3$ sintered under reducing conditions (Jugle, 1966) or in TiO_2 – excess materials sintered in an oxidizing atmosphere (*i.e.* in air; Lee *et al.*, 2000). The (111) twin boundaries are effectively stacking faults, where the oxygen octahedra become face-shared rather than corner-shared and the loss of oxygen is balanced locally by reducing Ti ions from 4+ to 3+ (Jugle, 1966; Eibl *et al.*, 1988). The local structure across the (111) twins in this work is similar to that of hexagonal $BaTiO_3$ in which octahedra are face shared in every third layer (Feteira *et al.*, 2006; Akimoto *et al.*, 1994). It is proposed that a similar twinning mechanism occurs in SRO, the signature of which is diffraction spots at $\pm1/3\{ooo\}$ and $\pm1/6\{ooo\}$ positions.

Perovskite structures can be described in terms of close-packed AO_3 layers with the *B*-site cations occupying the octahedral interstitials. In cubic perovskites, the AO_3 layers follow a stacking sequence of *ABCABC* (3*C* stacking) and the oxygen octahedra are corner-shared. Alternatively, when the AO_3 layers are at least partially packed in an *ABABAB* sequence, a hexagonal configuration results. In such a case, the oxygen octahedra are face-connected, which means fewer O atoms are needed to build up a three-dimensional network. A structure model for a simple (111) SRO twin boundary is proposed with reference to that for $BaTiO_3$ (Fig. 7; Jugle, 1966; Eibl *et al.*, 1988). The atoms at the twin boundary are arranged in a hexagonal rather than a cubic (3*C*) stacking sequence. Extending such a model to a general condition implies that

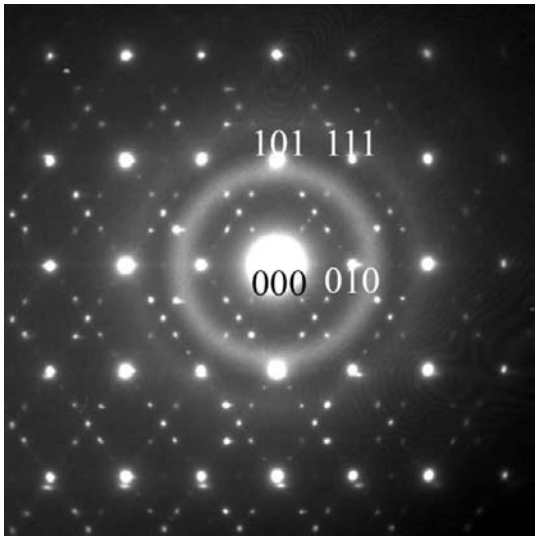

Figure 5
⟨110⟩ zone-axis diffraction pattern showing extra spots located along both the ⟨111⟩ pseudocubic directions.

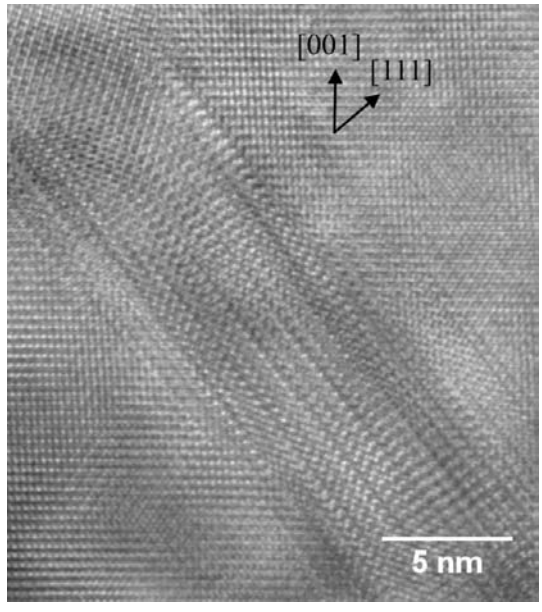

Figure 6
High-resolution TEM image showing a region containing stacking faults on (111) planes.

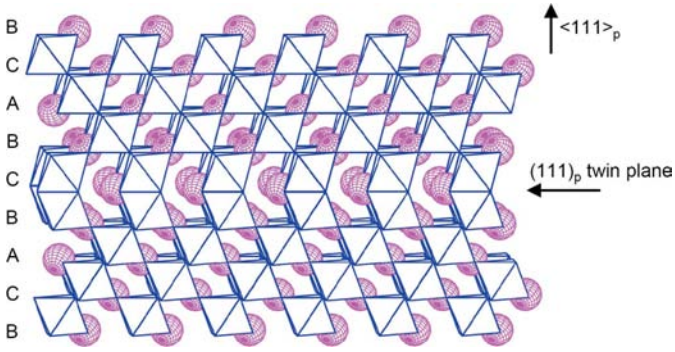

Figure 7
Schematic illustration of a structure model showing the face-shared oxygen octahedra at the (111) twin boundary in SRO thin films.

any interruption of the 3*C*-stacking sequence will result in local modifications from cubic to hexagonal.

Although the reason for the occurrence of a high density of (111) microtwins is unknown, it is plausible that the microtwins are stabilized by the $\sim 4.0\%$ lattice mismatch between SRO and LAO at the growth temperature. The formation of microtwins during epitaxial growth may help relieve misfit strain and would also accommodate any O non-stoichiometry such as is often present in vacuum-deposited thin oxide layers.

4. Conclusions

Extra reflections at $\pm 1/6(ooo)$ and $\pm 1/3(ooo)$ positions are present in electron-diffraction patterns from SRO grown on LAO substrates as a result of microtwinning on inclined $\{111\}_p$ planes. The extra reflections occur at commensurate positions and could be misinterpreted as arising from a more common perovskite superstructure associated with ordered $V_o^{\cdot\cdot}$ in combination with octahedral rotations or from a hexagonal perovskite lattice.

Financial support for this work is provided by the Engineering and Physical Science Research Council UK (EP/D067049/1G) and by the National Science Foundation (Materials World Network, DMR-0602770).

References

Ai, W. Y., Zhu, J., Zhang, Y., Li, Y. R., Liu, X. Z., Wei, X. H., Li, J. L., Zheng, L., Qin, W. F. & Liang, Z. (2006). *Appl. Surf. Sci.* **252**, 8326–8330.
Akimoto, J., Gotoh, Y. & Oosawa, Y. (1994). *Acta Cryst.* C**50**, 160–161.
Bachelet, R., Sanchez, F., Santiso, J. & Fontcuberta, J. (2008). *Appl. Phys. Lett.* **93**, 151916.
Chen, C. L., Cao, Y., Huang, Z. J., Jiang, Q. D., Zhang, Z., Sun, Y. Y., Kang, W. N., Dezaneti, L. M., Chu, W. K. & Chu, C. W. (1997). *Appl. Phys. Lett.* **71**, 1047–1049.
Chen, Y. X., Koike, J., Higuchi, T., Iwashita, S., Ishida, M. & Shimoda, I. (2002). *Philos. Mag. B*, **82**, 1731–1748.
Eibl, O., Pongratz, P. & Skalicky, P. (1988). *Philos. Mag. B*, **57**, 521–534.
Eom, C. B., Cava, R. J., Fleming, R. M., Phillips, J. M., Vandover, R. B., Marshall, J. H., Hsu, J. W. P., Krajewski, J. J. & Peck, W. F. (1992). *Science*, **258**, 1766–1769.
Fahey, K. P., Clemens, B. M. & Wills, L. A. (1995). *Appl. Phys. Lett.* **67**, 2480–2482.
Feng, Q. Q. & McConville, C. J. (2004). *J. Am. Ceram. Soc.* **87**, 2247–2251.
Feteira, A., Sinclair, D. C. & Reaney, I. M. (2006). *J. Am. Ceram. Soc.* **89**, 2105–2113.
Gan, Q., Rao, R. A., Eom, C. B., Garrett, J. L. & Lee, M. (1998). *Appl. Phys. Lett.* **72**, 978–980.
Glazer, A. M. (1972). *Acta Cryst.* B**28**, 3384–3392.
Herranz, G., Sanchez, F., Fontcuberta, J., Garcia-Cuenca, M. V., Ferrater, C., Varela, M., Angelova, T., Cros, A. & Cantarero, A. (2005). *Phys. Rev. B*, **71**, 174411.
Jiang, J. C. & Pan, X. Q. (2001). *J. Appl. Phys.* **89**, 6365–6369.
Jiang, J. C., Pan, X. Q. & Chen, C. L. (1998). *Appl. Phys. Lett.* **72**, 909–911.
Jugle, D. B. (1966). PhD thesis. Rensselaer Polytechnic Institute.
Keller, L. P. & Buseck, P. R. (1994). *Am. Mineral.* **79**, 73–79.
Kennedy, B. J. & Hunter, B. A. (1998). *Phys. Rev. B*, **58**, 653–658.
Krasevec, V., Drofenik, M. & Kolar, D. (1990). *J. Am. Ceram. Soc.* **73**, 856–860.
Lee, B. K., Chung, S. Y. & Kang, S. J. L. (2000). *J. Am. Ceram. Soc.* **83**, 2858–2860.
Lee, H. N., Christen, H. M., Chisholm, M. F., Rouleau, C. M. & Lowndes, D. H. (2004). *Appl. Phys. Lett.* **84**, 4107–4109.
Lee, H. N., Christen, H. M., Chisholm, M. F., Rouleau, C. M. & Lowndes, D. H. (2005). *Nature*, **433**, 395–399.
Levin, I., Bendersky, L. A., Cline, J. P., Roth, R. S. & Vanderah, T. A. (2000). *J. Solid State Chem.* **150**, 43–61.
Maria, J.-P., McKinstry, H. L. & Trolier-McKinstry, S. (2000). *Appl. Phys. Lett.* **76**, 3382–3384.
Maria, J. P., Trolier-McKinstry, S., Schlom, D. G., Hawley, M. E. & Brown, G. W. (1998). *J. Appl. Phys.* **83**, 4373–4379.
Oh, S. H. & Park, C. G. (2001). *J. Mater. Res.* **16**, 1998–2006.
Oh, S. H. & Park, C. G. (2004). *J. Appl. Phys.* **95**, 4691–4704.
Oppolzer, H. & Schmelz, H. (1983). *J. Am. Ceram. Soc.* **66**, 444–446.
Recnik, A., Bruley, J., Mader, W., Kolar, D. & Ruhle, M. (1994). *Philos. Mag. B*, **70**, 1021–1034.
Takahashi, K., Oikawa, T., Saito, K., Kaneko, S., Fujisawa, H., Shimizu, M. & Funakubo, H. (2002). *Jpn. J. Appl. Phys.* **41**, 5376–5380.
Vasco, E., Dittmann, R., Karthauser, S. & Waser, R. (2003). *Appl. Phys. Lett.* **82**, 2497–2499.
Wang, W. L. & Lu, H. Y. (2006). *Phys. Chem. Miner.* **33**, 435–444.
White, T. J., Segall, R. L., Barry, J. C. & Hutchison, J. L. (1985). *Acta Cryst.* B**41**, 93–98.
Woodward, D. I., Reaney, I. M., Yang, G. Y., Dickey, E. C. & Randall, C. A. (2004). *Appl. Phys. Lett.* **84**, 4650–4652.
Zakharov, N. D., Satyalakshmi, K. M., Koren, G. & Hesse, D. (1999). *J. Mater. Res.* **14**, 4385–4394.